Clim. Past Discuss., 10, 1223–1264, 2014
www.clim-past-discuss.net/10/1223/2014/
doi:10.5194/cpd-10-1223-2014

Climate of the Past Discussions
Open Access

Two distinct decadal and centennial cyclicities forced marine upwelling intensity and precipitation during the late Early Miocene in Central Europe

G. Auer[1], **W. E. Piller**[1], **and M. Harzhauser**[2]

[1]Institute for Earth Sciences, University of Graz, Heinrichstrasse 26, 8010 Graz, Austria
[2]Natural History Museum Vienna, Geological-Paleontological Department, Burgring 7, 1010 Vienna, Austria

Received: 4 March 2014 – Accepted: 19 March 2014 – Published: 28 March 2014

Correspondence to: G. Auer (gerald.auer@uni-graz.at)

Published by Copernicus Publications on behalf of the European Geosciences Union.

Abstract

Within a 5.5 m-thick succession of Upper Burdigalian (Karpatian) sediments in the North Alpine Foreland Basin (NAFB; Austria), dated to CNP-zone NN4, a high-resolution section was logged continuously. 100 samples were taken with a resolution of ~ 10 mm per layer and analysed using an integrated multi-proxy approach.

Earlier analyses of geochemistry and calcareous nannoplankton assemblages hint at small-scale, short-term variations in palaeoenvironmental conditions, such as water-column stratification, primary productivity, organic matter flux, bottom-water oxygenation, freshwater influx and changes in relative sea-level. The results indicate a highly dynamic shallow marine setting that was subject to high frequency environmental changes on a decadal to centennial scale.

Time-series analyses on nine different proxy-datasets using REDFIT-analysis and Wavelet spectra were applied to resolve a possible cyclic nature of these variations. Analyses revealed that different proxies for precipitation, upwelling intensity, and over all productivity likely were controlled by different cyclicities.

A best-fit adjustment of the likely sedimentation rates within the high-resolution section resulted in periodicities fitting well with the Lower (~ 65 yr) and Upper (~ 113 yr) Gleissberg cycle as well as the Suess/de Vries cycle (~ 211 yr). The section covers a timespan of ~ 1190 yr based on the correlation with solar cycles, which resulted in an estimated sedimentation rate of 575 mm kyr^{-1}.

For the first time, short-term climate variability on a decadal to centennial scale is resolved in Lower Miocene shallow marine laminated sediments in a land-based section. The results hint at a close relationship between climate variability and solar forcing during the Late Burdigalian. Moreover, accepting that these cyclicities are indeed of solar origin, this would indicate that precipitation was driven by the two Gleissberg cycles, while upwelling was driven by the Suess cycle. Furthermore, proxies for primary productivity were influenced by both cycles, although the Suess cycle exerts dominant control, reflecting a stronger influence of upwelling on primary productivity.

CPD
10, 1223–1264, 2014

1 Introduction

Instrumental documentation of high-frequency climate behaviour only reaches back several hundred years (see Le Treut et al., 2007 for an extensive discussion on the subject). Studying sediments offers a unique way to reconstruct climate variability in earth's past, also hinting at the processes influencing such changes. Astronomical parameters are a major force of climate change on different scales. On a centennial to decadal scale solar variation appears to be one of the key factors in determining the earth's climate (Patterson et al., 2004, 2013; Solanki et al., 2004; Gray et al., 2010;). While its causes are, for the moment, only poorly understood, solar activity clearly shows quasi-cyclic variances such as the 11 yr Schwabe-cycle, the 22 yr Hale-cycle, the 50–80 yr Lower Gleissberg-cycle, the 90–140 yr Upper Gleissberg-cycle, the ~ 210 yr Suess/de Vries cycle, and the 2200–2300 yr Hallstatt cycle, as well as unnamed cycles with a 500- and 1000 yr periodicity (see Kern et al., 2012, 2013 for discussion).

While cycles of solar origin are well documented in the Antarctic isotope record and ice cores (e.g., Damon and Sonett, 1991; Stuiver and Braziunas, 1993; Solanki et al., 2004), terrestrial and marine records around the globe also show evidence for solar cycles during the Quaternary (Stuiver and Braziunas, 1993; Stuiver et al., 1995; Taricco et al., 2009; Di Rita, 2013; Galloway et al., 2013). Comparable studies from the Neogene are scarce and mostly confined to warved (Lindqvist and Lee, 2009; Lenz et al., 2010) or laminated sediments of Miocene lakes (Gross et al., 2011; Kern et al., 2012, 2013; Harzhauser et al., 2013). These examples show clear evidence for solar cycles in the Miocene. However, studies of marine sediments on high-resolution short-term climate variability have never been conducted in pre-Pleistocene sediments.

Generally, only specific proxies are appropriate for this type of study. Besides geochemical and geophysical proxies, only microfossils occur in suitable quantities and are small enough to allow quantitative high-resolution studies on a sub-Milankovitch scale. Based on their small size, abundance and global distribution calcareous nannofossils are thus uniquely suited for such studies.

CPD
10, 1223–1264, 2014

While calcareous nannofossils are widely used in stratigraphy from the Mesozoic to recent, they are less often used for ecological studies, even though their ecological preferences are well documented. In particular, high-resolution studies using calcareous nannoplankton as a palaeoecological proxy have been mostly confined to the Pleistocene and Holocene (Negri and Giunta, 2001; Álvarez et al., 2005; Mertens et al., 2009; Incarbona et al., 2010). Even so, it has been proven, that calcareous nannofossils are strongly influenced by cyclic variations of the earth's climate, both on larger (Milankovich-) (Amore et al., 2012; Girone et al., 2013) and smaller scales. For the latter, influences related to solar variation were documented (Incarbona et al., 2010). Moreover, a tight relation to solar activity has to be expected for surface dwelling photosynthetic organisms.

All of these studies have been carried out on core samples, while calcareous nannofossils from Miocene surface outcrops have never been studied before on this resolution with a focus on the influence of solar variation on short-term climate variability.

A previous study conducted on finely laminated marine sediments of late Burdigalian age from the Central Paratethys already documented ecological variability on such a high-resolution during the late Early Miocene. A section was studied in terms of distribution of calcareous nannofossil assemblages, in combination with geochemical proxies. Based on this multi-proxy approach a clear link was shown between abundance distributions within the coccolith assemblages and changes in local environmental conditions, such as changes in relative sea-level, freshwater influx, nutrient availability and upwelling intensity (Auer et al., 2014).

This dataset has now been used to detect a possible cyclic nature in these changes and to correlate them with known decadal to centennial cycles of solar origin. Our results demonstrate that solar forcing had a strong influence on the local palaeoclimate and acted as a major pacemaker for the observed cyclic variations of the palaeoecological conditions within the area.

CPD
10, 1223–1264, 2014

2 Geological setting

The investigated outcrop is situated in a brickyard near Laa an der Thaya, roughly 50 km north of Vienna, Austria (48°43′0.84″ N, 16°24′45.18″ E; Fig. 1), where sediments of the Laa Formation are exposed. This Upper Burdigalian lithostratigraphic unit was deposited within the North Alpine Foreland Basin (NAFB), which was a part of the Central Paratethys during the Oligocene–Miocene (Harzhauser and Piller, 2007; Piller et al., 2007).

The Laa Formation corresponds to the lower to middle Karpatian (17.2–16.5 Myr; Dellmour and Harzhauser, 2012) of the regional chronostratigraphic scheme of the Central Paratethys. Grunert et al. (2012, 2010b) suggest a total range of 17.2 to 15.9 Ma for the Karpatian (Fig. 2). Seismic logs indicate a maximum thicknesses of up to 1000 metres for the Laa Formation, which displays a general coarsening upward trend (Roetzel and Schnabel, 2002; Adamek et al., 2003; Dellmour and Harzhauser, 2012).

The Laa Formation is composed of marine, calcareous, laminated, greenish to brownish grey, micaceous silty clays with thin fine sand intercalations that unconformably overly Ottnangian sediments (Nehyba and Petrová, 2000; Roetzel and Schnabel, 2002; Adamek et al., 2003).

Palaeoenvironmental reconstructions suggest an inner to outer shelf environment of 100 to 200 m water depth, with dysoxic bottom water conditions, based on benthic foraminiferal assemblages (Spezzaferri and Ćorić, 2001). Roetzel and Schnabel (2002) interpreted frequently occurring sandy intercalations as episodic storm events. Assemblages of calcareous nannoplankton point towards cool to temperate, nutrient rich surface water conditions, and local upwelling (Spezzaferri and Ćorić, 2001). Similar upwelling conditions were also reported from other locations within the NAFB during the Early Miocene (Spezzaferri et al., 2002; Roetzel et al., 2007; Grunert et al., 2010c, 2012).

CPD
10, 1223–1264, 2014

Nannofossil assemblages place the Laa Formation entirely into Neogene Nannoplankton Zone NN4 of Martini (1971) (Spezzaferri and Ćorić, 2001; Spezzaferri et al., 2002; Adamek et al., 2003; Svabenicka et al., 2003), or alternatively into Mediterranean Neogene Nannoplankton zone MNN4a (Fornaciari and Rio, 1996; Fornaciari et al., 1996) and also Calcareous Nannofossil Miocene zone CNM6 of Backman et al. (2012) (Auer et al., 2014). The assemblages are generally of low to moderate diversity with high amounts (up to 45 %) of reworked (Paleogene and Cretaceous) specimens (Auer et al., 2014).

3 Material and methods

3.1 Sampling and field methods

In the clay pit a 5.5 m-thick succession of finely laminated blue-grey to green-grey clays with intercalated silt and fine sand layers is exposed. The laminated clays show variable thicknesses on a sub-millimetre to centimetre scale. The sand layers, reaching a thickness of up to 5 cm, decrease in frequency towards the top of the succession, and show well-preserved current ripples. The exposed sediments are mostly free of bioturbation as well as macrofossils.

Besides lithological logging, natural gamma radiation and magnetic susceptibility were measured using a portable scintillation counter (Heger–Breitband–Gammasonde) and a portable magnetic susceptibility meter (Exploranium KT-9) respectively.

Within this succession, a high-resolution sub-section with a total thickness of 940.5 mm was logged, composed of finely laminated clays with some intercalations of fine sand and silt. The sub-section starts at 3.06 m above the base of the section and contains 100 layers with a thickness of ~ 10 mm, that were continuously sampled using a top-down approach (Auer et al., 2014).

CPD
10, 1223–1264, 2014

In the lower half of the section the clay is clearly laminated. Lamination becomes less pronounced towards the top while sandy/silty intercalations increase in frequency. This general coarsening upward trend is also reflected in the geophysical measurements. Furthermore, the lower boundaries of the layers become less clearly defined and increasingly wavy. Bioturbation only occurs in two successive layers close to the base of the section (Fig. 3).

3.2 Sample preparation and treatment

For geochemical analysis approximately 0.1–0.15 g of powdered sediment of all 100 samples were analysed in a LECO CS230 analyser in order to determine the wt. % of total carbon (TC), total organic carbon (TOC) and sulphur. The content of total inorganic carbon (TIC) was then calculated based on TC and TOC content (TIC = TC – TOC). Using the stoichiometric formula (8.34 × TIC) the calcium carbonate content was also calculated (Stax and Stein, 1995; Grunert et al., 2010a). The ratio of organic carbon to sulphur was calculated after Berner and Raiswell (1984).

For analyses of the calcareous nannofossil assemblages smear slides of the samples were prepared after the standard preparation methods outlined in Bown and Young (1998). Samples were not treated beforehand in order to preserve the original assemblage and ultrasonicated for 5 s in order to facilitate a better disarticulation of the sediment before transferring the suspension onto a cover slip. The slides were mounted using Eukitt®, before being studied under a standard light microscope with a magnification of 1000X under parallel and crossed nicols. For quantitative analyses of the assemblages in terms of abundance and distribution approximately 300 specimens were counted within each sample and identified to species level.

3.3 Taxonomic remarks

Calcareous nannoplankton assemblages were identified using the Nannotax website (Young et al., 2013) in combination with the taxonomy of Perch-Nielsen (1985b, a),

CPD
10, 1223–1264, 2014

Young (1998), Varol (1998), and Brunette (1998), supplemented by the Handbook of Calcareous Nannoplankton 1–5 (Aubry, 1984, 1988, 1989, 1990, 1999). The revised taxonomy for the Paratethys published by Galović and Young (2012) was also taken into consideration.

Recorded taxa were first identified to species level and then grouped according to their stratigraphic range, in order to quantify the amount of allochthonous taxa present within the assemblages, and also to create a stratigraphic framework for the section.

For the genus *Reticulofenestra* the standard size definition of Young (1998) was used: *Reticulofenestra minuta* < 3 µm, *R. haqii* 3–5 µm, *R. pseudoumbilicus* > 5 µm. The distinction of medium sized reticulofenestrids based on their central area (*R. haqii*, open; *R. antarctica*, closed) (e.g., Wade and Bown, 2006) was not used in this study.

A total of 124 calcareous nannofossil taxa were identified. Out of which 24 occur within nannoplankton zone NN4 and represent an average of 67.86 % ($\sigma = 5.33$) of the total assemblage. The autochthonous assemblage includes 5 taxa with an average abundance of > 1 % (see Table 1, Auer et al., 2014). Many of these taxa have a wide stratigraphic range and partial reworking cannot be excluded for certain taxa (e.g., *Coccolithus pelagicus*, *Cyclicargolithus floridanus*, *Sphenolithus moriformis* and *Reticulofenestra minuta*). These taxa were considered as entirely autochthonous, since reworked specimens could not be distinguished from autochthonous ones. Nevertheless, statistical analysis and palaeoecological reconstructions support that a primary ecological signal is preserved within the assemblage, despite likely partial reworking (Auer et al., 2014).

The remaining 100 taxa are all clearly allochthonous of both Paleogene and Cretaceous age. 41 taxa can be attributed to mainly Paleocene and Eocene ages. The Cretaceous assemblage is represented by 59 taxa of mainly Campanian to Maastrichtian age. All 100 taxa of the allochthonous assemblages were grouped together and used as a proxy for terrigenous input in subsequent analyses (Auer et al., 2014).

CPD
10, 1223–1264, 2014

3.4 Statistical treatment

Since any observed abundance of calcareous nannoplankton is not normally distributed the counts were transformed using the arcsine-transformation, as outlined in Sokal and Rohlf (1995). The reason for using a transformation was to create a more normally distributed dataset that is better suited for the subsequent analyses.

Spectral analyses of geochemical and palaeobiological datasets were performed using the REDFIT tool of the PAST statistics package (Hammer et al., 2001). The REDFIT-analysis was selected based on the fact that REDFIT was specifically designed to handle unevenly spaced noisy data (Schulz and Mudelsee, 2002). This made the method ideal for the analysis of datasets based on layers of varying thickness.

Prior to analysis the samples were evaluated based on their sedimentological, geochemical and taphonomic characteristics and separated into 3 depositional intervals (Figs. 4 and 5). Based on this simple evaluation the topmost 30 samples of the section were excluded based on intercalations of coarser sediment indicating changes in the sedimentation rate (Figs. 4 and 5). Such disturbances in the rate of sedimentation are usually detrimental to the detection of clear signals of periodic cycles in the section (Weedon, 2003). For the remaining 70 samples, with an overall thickness of 684 mm, a continuous sedimentation rate was assumed (Figs. 4 and 5).

In order to consider also the thickness of the sampled layers, two data points were used for each sample. One data point was set at the bottom and one at the top of the layer. This was done to express each sample as a continuous layer instead of one single data point. In total, 9 datasets (3 geochemical and 6 based on coccolith abundance data) were analysed using REDFIT. The five autochthonous coccolith taxa used, were selected due to their high abundance and specific ecological preferences. The amount of allochthonous taxa was used as a proxy for terrigenous input.

For the calculation of the REDFIT periodograms, different windows as well as segmentations and oversampling rates were applied to all datasets (see Table 2). This was

CPD
10, 1223–1264, 2014

done in order to achieve clear peaks in the periodograms for each separate dataset (Hammer, 2010).

After performing the REDFIT-analysis on the datasets of all relevant samples, a Monte-Carlo simulation was performed on the resulting power-spectra in order to test the time series under white-noise conditions before examination of significant peaks (Hammer et al., 2001; Hammer, 2010).

In order to eliminate any artificial peaks created by the REDFIT-analysis, the Nyquist frequency was used. The Nyquist frequency is the highest possible frequency in a sampled set that can be expressed by a simple sine or cosine wave, and is generally assumed to be a frequency of twice the average sampling distance (Weedon, 2003). The Nyquist frequency is calculated using the reciprocal value of the total thickness of the section (684 mm) divided by twice the amount of used samples (70). The Nyquist frequency for the studied high-resolution section can thus be calculated as $1/(684/(70\times 2))$. This calculation yields a value for the highest possible frequency that is not an artefact created by the REDFIT method as $f = 0.051$. This translates into a periodicity of about 19.6 mm.

Below this threshold periodicities are assumed to be artefacts and were excluded from subsequent analysis. Weedon (2003) actually suggests a minimal spacing of 4 samples per sinusoid, which effectively would double the minimal periodicity of cycles to roughly 39 mm. For our analysis we also considered periodicities of 25 to 30 mm as viable, because of the fact that the Nyquist frequency is based on average sample spacing, but our samples cover variable thicknesses and are often thinner than the calculated average thickness of 9.77 mm.

Additionally, any frequencies above a periodicity larger than half the total thickness of the section (342 mm) were also considered to be of insufficient significance to safely assume the presence of those periodicities. Therefore all frequency components below $f = 0.003$ were also excluded.

An automatic linear interpolation was used to create datasets with 1000 new evenly spaced data-points without compromising the shape of the original curve. These

CPD
10, 1223–1264, 2014

datasets were used for methods (filtering and Wavelet-analyses) that require evenly spaced datasets.

Significant periodicities, as detected by the REDFIT periodograms, were filtered using Gaussian band-pass filter in the application Analyseries (Paillard et al., 1996). The method selects only the desired frequency components of a given data set and displays its amplitude, while removing all other frequencies. To encompass the whole range of the selected frequencies a bandwidth with the size of 25 % of the frequency was applied to all Gaussian band-pass filters. Band-pass filtering is now standard practice for modern cyclostratigraphy, since it allows for a better examination of the varying degrees of influence the detected frequencies have over a time interval (Weedon, 2003).

To further evaluate any found and filtered periodicities Wavelet analyses were also performed on all investigated datasets using the corresponding tool from the PAST statistics package (Hammer, 2010; Hammer et al., 2001). Wavelet spectra allow the simultaneous graphic examination of all found frequencies in combination with their amplitude at each data-point of a given dataset. This method was developed to accurately trace possible frequency and amplitude modulations of detected periodicities throughout a time series (Hammer et al., 2001; Hammer, 2010).

4 Results

4.1 Time series analyses

For the detection of possible cyclicities in the high-resolution section 9 relevant datasets were selected for the REDFIT-analysis (Fig. 6). These datasets include geochemical (calcium carbonate, sulphur, total organic carbon; Table 1) and palaeobiological proxies, with the 5 autochthonous taxa > 1 %, as well as allochthonous taxa (Table 1). The detected frequencies and periodicities for the 9 datasets are shown in Table 3. Detailed descriptions of the periodicities, variations in the filtered amplitudes as well as the cor-

CPD
10, 1223–1264, 2014

relation with the Wavelet analyses are given for each respective dataset in the following section:

Calcium carbonate displays significant peaks at periodicities of 91.84 and 153.08 mm, as well as 38.81 and 30.96 mm. The relative proximity of the latter two periodicities indicates that they may represent two different frequency components of the same periodicity, and were therefore considered further (Fig. 7). Filtering indicates that the 91.84 mm periodicity has an amplitude modulation indicative of a very strong influence in the middle and upper part of the section (Fig. 7a). This pattern hints at a steady increase in influence over the section. The amplitude modulation for the 153.08 mm periodicity reveals an increase in the mid-part of the section where it nearly doubles in intensity, staying constant until the top of the section (Fig. 7a). The two periodicities of lower significance (38.81 and 30.96 mm) show a remarkably similar amplitude modulation over the section, further hinting at their close relationship to each other. Their influence dominates the lower part of the section, which is followed by a strong decline, before increasing in amplitude synchronously with the 91.81 mm periodicity, followed by a gradual decline towards the top of the section (Fig. 7a). The Wavelet-analysis also supports the filtered periodicities detected by REDFIT. Other frequencies not detected by the REDFIT-analysis also occur in the Wavelet but were thus not considered significant (Fig. 7a).

Sulphur yields two peaks at periodicities of 125.25 and 44.44 mm respectively. Another less significant peak occurs at a periodicity of 36.26 mm (Fig. 6). Applying a Gaussian filter to the periodicities revealed, that the 125.25 mm periodicity dominates the lower part of the section, but is much less pronounced in the middle and upper part. The two higher periodicities of 44.44 and 36.26 mm show an inverse pattern. They also show a similar pattern in amplitude modulation over time, hinting at a close relationship between them (Fig. 7b). The Wavelet-analysis also supports the periodicities detected by REDFIT (Fig. 7b).

TOC reveals two peaks at periodicities of 119.8 and 33.2 mm (Fig. 6). Applying a Gaussian filter reveals amplitudes for the 119.8 mm periodicity that are lower at the

CPD
10, 1223–1264, 2014

bottom of the section but increase towards the top. The 33.2 mm periodicity exhibits generally lower amplitudes over most of the section, and only increases close to the top (Fig. 7c). Both frequencies are well represented in the Wavelet analysis, although they show a slight spread. This implies that periodicities detected by REDFIT may be subject to a slight variability over time (Fig. 7c).

Coccolithus pelagicus displays three significant peaks at periodicities of 275.54, 119.8 and 58.63 mm respectively (Fig. 6). The amplitudes for the 275.54 mm periodicity display a constant decrease towards the top of the section. The 119.8 mm periodicity increases in amplitude towards a maximum in the upper middle part of the section before decreasing slightly towards the top. The periodicity of 58.63 mm shows much more variable amplitudes. Amplitude maxima for this periodicity are located at the bottom and top of the section with lower amplitudes in the middle part. A slightly less pronounced increase in amplitude can also be detected in the upper middle part of the section (500 to 550 mm; Fig. 8a). All frequencies detected by the REDFIT-analysis are represented in the wavelet analysis and also correlate with the filtered amplitudes (Fig. 8a).

Cyclicargolithus floridanus only exhibits a single peak with a periodicity of 229.61 mm (Fig. 6). The filtering reveals constantly increasing amplitudes throughout the section (Fig. 8b). The wavelet analysis also shows the 229.61 mm periodicity with a significant intensity (Fig. 8b). Additionally, other frequencies appear in the wavelet analysis. Although not significant, they show a striking similarity to periodicities observed within the 8 other proxies.

Reticulofenestra haqii has two peaks with periodicities of 65.14 and 42.41 mm (Fig. 6). Filtering reveals rather low amplitudes for the 65.14 mm periodicity, with a single strong excursion centred on sample 66. The 42.41 mm periodicity increases in amplitude in the lower part of the section, remains rather constant to sample 39, but vanishes nearly completely above (Fig. 8c). The wavelet diagram shows a good correlation between the detected intensities of the periodicities (Fig. 8c).

Reticulofenestra minuta exhibits strikingly similar periodicities to *R. haqii* with peaks at 65.14 and 42.74 mm (Fig. 6). Filtering shows that the 65.14 mm periodicity shows

CPD
10, 1223–1264, 2014

strongly varying amplitudes with excursions at the bottom and very top of the section. Highest amplitudes are located at an excursion in the middle part centred at sample 66. The 42.74 mm periodicity remains constantly low in amplitudes with only a short increase from sample 50 up to 35. At the top it vanishes nearly completely (Fig. 8d). The calculated wavelet diagram corresponds well with the detected frequencies (Fig. 8d).

Reticulofenestra pseudoumbilicus reveals two peaks with periodicities of 172.21 and 25.51 mm. Another distinct but not significant peak appears at a periodicity of 57.41 mm (Fig. 6). Filtering shows increasing amplitudes for the 172.21 mm periodicity peaking at sample 48, and a decrease towards the top. The 25.51 mm periodicity displays highly fluctuating amplitudes throughout the section, with a maximum centred on sample 49 (Fig. 8e). The 57.41 mm periodicity shows constantly low amplitudes that nearly vanish for a short period in the middle part of the section (Fig. 8e).

The allochthonous taxa show three peaks with periodicities of 77.61, 45.28 and 36.22 mm (Fig. 6). Filtering the periodicities reveals that the 77.61 mm periodicity exhibits quite low amplitudes in the lower part of the section, before increasing at sample 80. Following this increase the amplitude remains constant throughout the section. The two remaining periodicities show similar amplitude modulations throughout the section. They exhibit rather low amplitudes with a single excursion detected between sample 91 and 65 (Fig. 8f). The wavelet correlates well with the periodicities detected by REDFIT (Fig. 8f).

5 Discussion

5.1 Age–depth model

Using the average sedimentation rate calculated for the basinal parts of the Central Paratethys based on the cross-correlation of insolation cycles by Hohenegger and Wagreich (2011) as a rough baseline for this hypothesis, a sedimentation rate of 512 mm kyr^{-1} was assumed.

CPD
10, 1223–1264, 2014

Applying this sedimentation rate to the 684 mm gives a rough estimate of 1335 yr for the section. If the same rate of sedimentation is now applied to the periodicities in mm that were calculated by REDFIT- and Wavelet-analyses, they can simply be translated from cycles based on thickness into time-based cyclicities (Figs. 7 and 8; Table 3).

Organizing those results reveals that most detected cycles can be roughly arranged into groups of similar periodicities: the first group encompasses all periodicities below 65 yr and thus contain three periodicities: 60.47 yr (calcium carbonate), 64.84 yr (TOC) and 48.83 yr (*Reticulofenestra pseudoumbilicus*). The second group ranges between 70 and 80 yr and encompasses three periodicities. 75.8 yr (calcium carbonate), 70.81 (sulphur) and 70.74 yr (allochthonous taxa). A third group is formed by periodicities ranging between 80 and 90 yr, including four periodicities: 86.8 yr (sulphur), 82.83 yr (*Reticulofenestra haqii*), 83.48 yr (*Reticulofenestra minuta*) and 88.43 yr (allochthonous taxa). A fourth group can be formed with four periodicities between 110 and 130 yr. The group contains: 114.51 yr (*Coccolithus pelagicus*), 127.33 yr (*Reticulofenestra haqii*), 127.23 yr (*Reticulofenestra minuta*) and 112.12 yr (*Reticulofenestra pseudoumbilicus*). The two slightly more isolated periodicities of 151.58 yr (allochthonous taxa) and 179.38 yr (calcium carbonate) were also grouped. Another group of three periodicities forms around an average of 237.53 yr, and encompasses the periodicities 244.62 yr (sulphur), 233.98 yr (TOC) and 233.99 yr (*Coccolithus pelagicus*). Two other periodicities appear at 298.98 yr (calcium carbonate) and 336.35 yr (*Reticulofenestra pseudoumbilicus*) and form an average of 317.67 yr. The last two remaining periodicities appear to be completely separated at 448.46 yr (*Cyclicargolithus floridanus*) and 538.16 yr (*Coccolithus pelagicus*). Comparing the detected periodicities with known cycles linked to solar variation, such as the Gleissberg (Wolf, 1892; Gleissberg, 1939; Ogurtsov et al., 2002) and Suess/de Vries cycles (Damon and Sonett, 1991; Stuiver and Braziunas, 1993; Wagner et al., 2001) shows a clear correlation. For instance, the Gleissberg cycle is split into two distinct frequency components, centered on 50–80 yr and 90–140 yr (Ogurtsov et al., 2002). The Suess/de Vries cycle centres on a periodicity of 208 yr and is well documented in Holocene (Schimmelmann et al., 2003; Yin

CPD
10, 1223–1264, 2014

et al., 2007; Raspopov et al., 2008; Taricco et al., 2009; Incarbona et al., 2010; Kern et al., 2012, 2013; Di Rita, 2013; Galloway et al., 2013) and Late Miocene (Pannonian) records (Kern et al., 2012, 2013). Comparing the average age ranges of the detected periodicity groups with the known ranges for both the Gleissberg and Suess/de Vries cycle, shows that nearly all values are slightly higher than the known periodicities of the established cycles. Since all cycles appear to be consistently higher, it can be assumed, that the estimated sedimentation rate of 512 mm kyr^{-1} is to low. Increasing the sedimentation rate to a value of 575 mm kyr^{-1}, which is well within the recorded ranges of the North Alpine Foreland Basin, would lower the recorded periodicities to values that fit closely to known cycles.

Corresponding rates of sediment accumulation have been reported from recent shallow marine areas such as the western Adriatic Sea (Frignani et al., 2005) and the Mediterranean continental margin (Sanchez-Cabeza et al., 1999). Similarly, the Santa Barbara Basin shows high rates of sediment accumulation (often reaching 1.4 mm yr^{-1}), anoxic conditions and high primary productivity (Stein and Rack, 1992; Behl, 1995; Thunell et al., 1995).

After correcting the sedimentation rate accordingly, the recalculated time values of the periodicities now fit very well within the reported frequency ranges for both the Upper and the Lower Gleissberg cycle, as well as the Suess/de Vries cycle. Calculating the average of all values that lie within the particular ranges of the cycle gives mean values of 127.22 yr for all periodicities associated with the Upper Gleissberg cycle and an average of 64.17 yr for the Lower Gleissberg cycle. Similarly, the average of periodicities associated with the Suess/de Vries cycle now average at 211.5 yr (Table 3).

Likewise, the 399.32 yr periodicity fits well with a reported 400 yr cycle that was detected in multiple studies of both marine and lacustrine sediments from the Holocene (Dean and Schwalb, 2000; Domack et al., 2001; Dean et al., 2002). The detected periodicity of 479.20 yr (275.54 mm) may be loosely linked to an unnamed 500 yr cycle (Stuiver et al., 1995; Chapman et al., 2000). Yin et al. (2007) and Kern et al. (2012)

CPD
10, 1223–1264, 2014

detected comparable periodicities related to this cycle in Holocene and Late Miocene records (Table 3).

The detection of cycles with higher frequencies, like the well known ~ 11 yr sunspot or Schwabe cycle (Schwabe and Schwabe, 1844), as well as the closely related ~ 22 yr Hale cycle, was inhibited by the sample spacing, as one sample is roughly equivalent to a time of 15 yr in our current model. Furthermore, the Nyquist-frequency, which is the theoretical limit, stating that a sinusoidal curve can only be expressed by at least 2 samples, making any cycle below ~ 34 yr impossible to detect in our material (Weedon, 2003). Most cycles are far above the significance threshold of 4 samples per sinusoid (~ 68 yr), recommended by Weedon (2003).

5.2 Time estimates

Based on the remarkably close fit of detected periodicities with previously reported cycles of solar variation in both Holocene and Late Miocene sediments, it can be assumed that the total time represented in the 684 mm of the high-resolution section of Laa an der Thaya accounts for roughly 1190 yr. Assuming that the sedimentation rate did not change significantly over the total 5.5 m section in the clay pit of Laa an der Thaya it would therefore contain a total of ~ 9565 yr.

5.3 Ecological interpretation

While all studied proxies appear to be influenced by cycles related to solar forcing, their individual response varies. Significant frequencies are present in most proxies, the intensity of their response, however, differs from each other. This seems to indicate that different solar cycles are expressed in a unique way in each proxy. Kern et al. (2012, 2013) came to a similar conclusion based on their study of Late Miocene lake sediments. A closer cross-examination of the periodicities in all studied proxy-data reveals striking similarities in the periodicities for proxies linked to the same environmental parameters. This coupled response of different, unrelated proxies for the same

CPD
10, 1223–1264, 2014

environmental parameters strongly hints at a preservation of a cyclic climate variation within these proxies linked to solar variation.

One such similarity is the strong evidence of the ~ 208 yr Suess/de Vries cycle in TOC and *Coccolithus pelagicus*, with a similar peak in sulphur. TOC is considered a good indicator for primary productivity in the oceans (Rohling, 1994; Vilinski and Domack, 1998; Kuypers et al., 2004; Meyers and Arnaboldi, 2005). *Coccolithus pelagicus* is generally regarded a coccolith species that blooms during times of high fertility, especially in upwelling environments. The content of sulphur in the sediment is a good indicator for dysoxic to anoxic bottom water conditions, which usually occur when input of organic matter into the sediment is increased due to high primary productivity (Berner, 1981; Maynard, 1982; Berner and Raiswell, 1984). Comparing these factors with a similar peak pattern in the REDFIT-analysis points towards an influence of the Suess/de Vries cycle on primary productivity, oxygen content and the abundance of *C. pelagicus*. This further indicates that locally confined upwelling was strongly dependent on a ~ 208 yr cyclicity forced by solar variation. Similar relationships between upwelling and cycles of solar variation have been found in previous studies for the Holocene (Santos et al., 2011).

A link between the major periodicities detected for the calcium carbonate content and the amount of allochthonous taxa suggests that the calcium carbonate content in the section was strongly influenced by the terrigenous input into the sediment. Since coccolitophores produced more massive coccoliths during the Cretaceous (Stanley et al., 2005), compared to Early Miocene coccolith taxa, allochthonous taxa have a significant contribution to the calcium carbonate content. The similarities between the content of allochthonous taxa and calcium carbonate can thus be seen as an expression of changing terrigenous input caused by variations in precipitation. Consequently, our analyses show that precipitation was strongly influenced by the Upper (~ 90–140 yr) and Lower (~ 50–80 yr) Gleissberg cycle.

The abundance of *Reticulofenestra* in the section also reveals a strong influence by both the Upper and Lower Gleissberg cycle. All Early Miocene taxa of this genus are

CPD
10, 1223–1264, 2014

generally associated with raised nutrient levels of terrestrial origin (Okada and Honjo, 1973; Haq, 1980; Aubry, 1992; Flores et al., 1995; Okada and Wells, 1997; Wade and Bown, 2006). Since the amount of terrigenous nutrients is principally influenced by the amount of precipitation in the hinterland, a link between precipitation and solar activity seems likely. A complex link between cosmic rays emitted by the sun and the amount of cloud cover was previously discussed (e.g., Svensmark and Friis-Christensen, 1997; Kristjánsson et al., 2004; Erlykin et al., 2010). Although the link seems tenuous at best, our findings appear to be in agreement with this assumption.

The fluctuations in nutrient availability also become apparent in the sulphur content, since the amount of sulphur is directly linked to lowered oxygen conditions at the sea floor caused by increased primary productivity as a result of higher fertility levels through terrigenous influx.

The influence of solar forcing that affected different ecological parameters also becomes apparent in a direct comparison of the filtered amplitudes in the studied proxies and the palaeoenvironmental reconstruction based on geochemical analyses and calcareous nannoplankton assemblages of Auer et al. (2014). A shift in amplitude occurs in some parameters that corresponds well with the observed changes of palaeoenvironmental conditions from a more near-shore freshwater influenced setting in the lower part, compared to the more upwelling dominated part in the upper part of the studied section. This shift is clearly visible in the Wavelet spectra of sulphur and TOC contents, as well as the relative abundances of *Coccolithus pelagicus*. Amplitudes of these proxies are generally lower in the lower part compared to the upper part, indicating that a setting closer to the shore is subject to a stronger overprint of solar variation in the ecological signal compared to a more distal setting.

Conversely, proxies with a strong connection to precipitation, freshwater influx and terrigenous nutrient input, such as calcium carbonate content, *Reticulofenestra haqii, R. minuta*, *R. pseudoumbilicus* and the amount of allochthonous taxa, seem to be much less influenced by this shift in the depositional environment, indicating that the influence

CPD
10, 1223–1264, 2014

of terrigenous input remained constant throughout the section, while upwelling only occurred in the more distal setting, which influenced the upper part of the section.

6 Conclusions

The cyclic nature of climatic changes preserved in a total of nine geochemical and palaeoecological proxies was studied using time series analysis (REDFIT-analysis and Wavelet spectra). All proxies display highly similar periodicities, although some variations in power and their exact location within the frequency band occur. Our results expand on a previous study focussed on changes in palaeoenvironmental conditions caused by changes in relative sea-level (Auer et al., 2014) and reveal a strong influence of small-scale short-term climate variability on local palaeoenvironmental conditions, caused by cyclic variations in solar activity.

Using a best-fit adjustment of established sedimentation rate estimates defined for the basinal parts of the Paratethys, the detected periodicities correspond remarkably well with cycles of solar variation present in Holocene sun spot records. Consequently, the section appears to be influenced by the Lower (~ 65 yr) and Upper (~ 113 yr) Gleissberg cycle, as well as the 211 yr Suess/de Vries cycle. Other reported solar cycles of ~ 400 yr and ~ 500 (~ 480) yr are also represented but less significant. Best-fit adjustment of sedimentation rates resulted in an estimated 575 mm kyr^{-1} for the high-resolution section, resulting in a timespan of ~ 1190 yr for the 684 mm thick section.

Accepting the hypothesis that these cycles represent environmental responses to known solar cycles, the integrated investigation of multiple palaeoenvironmental proxies revealed a complex interplay of solar variation with the environment (Fig. 9). While variations in coccolith abundances and geochemical data show a clear correlation to the calculated solar cycles, their response to different cycles varies considerably. Similar responses to solar forcing were found within proxies related to the same ecological parameters indicating that the observed cyclicities represent a clear influence of solar forcing on climatic conditions. Based on this, we found that the Upper and Lower

CPD
10, 1223–1264, 2014

Gleissberg cycles appear to be a driving factor for the amount of terrigenous influx into the ocean and thus precipitation or wind. This link is reflected in the amount of allochthonous taxa, a direct proxy for terrigenous input, and also the abundance of reticulofenestrids, a proxy for freshwater influx and availability of terrigenous nutrients. This suggests that precipitation rather than wind was the key factor (Fig. 9). Upwelling conditions and water temperature, in turn were controlled by the longer Suess/de Vries cycle, reflected in a similar response of *Coccolithus pelagicus*, a typical tracer for upwelling fronts (and thus coastal wind systems) and cooler SSTs (Fig. 9). TOC and sulphur, both indicators of increased primary productivity and anoxic bottom water conditions, often associated with high primary productivity were conversely influenced by both cyclic systems, reflecting organic matter flux from both terrigenous nutrients and upwelling driven primary productivity (Table 1; Figs. 6, 7 and 9).

Supplementary material related to this article is available online at http://www.clim-past-discuss.net/10/1223/2014/cpd-10-1223-2014-supplement.zip.

Acknowledgements. The authors would like to thank Stjepan Ćorić (Geological Survey of Austria, Vienna), Patrick Grunert (University of Graz) and Andrea Kern (State Museum of Natural History Stuttgart) for many helpful comments and discussions. We also would like to thank Marie-Pierre Aubry (Rutgers University), for providing key literature. Additional thanks go to the participants of the field-course "Paleontological Lab- and Fieldwork" for their help with sampling and the logging of the outcrop and David Strahlhofer (University of Graz) for his assistance with sample preparations in the lab. Funding for this study was provided by the FWF (grant P-23492-B17).

References

Adamek, J., Brzobohaty, R., Palensky, P., and Sikula, J.: The Karpatian in the Carpathian Foredeep (Moravia), in: The Karpatian – a Lower Miocene Stage of the Central Paratethys, edited by: Brzobohaty, R., Cicha, I., Kovác, M., and Rögl, F., 75–89, Masaryk University, Brno, 2003.

CPD
10, 1223–1264, 2014

Amore, F. O., Flores, J. A., Voelker, A. H. L., Lebreiro, S. M., Palumbo, E., and Sierro, F. J.: A Middle Pleistocene Northeast Atlantic coccolithophore record: paleoclimatology and paleoproductivity aspects, Mar. Micropaleontol., 90–91, 44–59, doi:10.1016/j.marmicro.2012.03.006, 2012.

Aubry, M.-P.: Handbook of Cenozoic Calcareous Nannoplankton: Book 1, Ortholithae (Discoasters), Micropaleontology Press, New York, 1984.

Aubry, M.-P.: Handbook of Cenozoic Calcareous Nannoplankton: Book 2, Ortholithae (Holococcoliths, Ceratoliths, Ortholiths and Others), Micropaleontology Press, New York, 1988.

Aubry, M.-P.: Handbook of Cenozoic Calcareous Nannoplankton: Book 3, Ortholithae (Pentaliths, and Others), Heliolithae (Fasciculiths, Sphenoliths and Others), Micropaleontology Press, New York, 1989.

Aubry, M.-P.: Handbook of Cenozoic Calcareous Nannoplankton: Book 4, Heliolithae (Helicoliths, Cribriliths, Lopadoliths and Others), Micropaleontology Press, New York, 1990.

Aubry, M.-P.: Late Paleogene calcareous nannoplankton evolution: a tale of climatic deterioration, in: Eocene–Oligocene Climatic and Biotic Evolution, edited by: Prothero, D. R. and Berggren, W. A., Princeton University Press, New Jersey, 272–208, 1992.

Aubry, M.-P.: Handbook of Cenozoic Calcareous Nannoplankton, Book 5: Heliolithae (Zygoliths and Rhabdoliths), Micropaleontology Press, New York, 1999.

Auer, G., Piller, W. E., Harzhauser, M.: High-resolution calcareous nannoplankton palaeoecology as a proxy for small-scale environmental changes in the Early Miocene, Mar. Micropaleontol., in review, 2014.

Álvarez, M. C., Flores, J. A., Sierro, F. J., Diz, P., Francés, G., Pelejero, C., and Grimalt, J. O.: Millennial surface water dynamics in the Ría de Vigo during the last 3000 yr as revealed by coccoliths and molecular biomarkers, Palaeogeogr. Palaeoclimatol. Palaeoecol., 218, 1–13, doi:10.1016/j.palaeo.2004.12.002, 2005.

Backman, J., Raffi, I., Rio, D., Fornaciari, E., and Pälike, H.: Biozonation and biochronology of Miocene through Pleistocene calcareous nannofossils from low and middle latitudes, Newsl. Stratigr., 45, 221–244, doi:10.1127/0078-0421/2012/0022, 2012.

Behl, R. J.: Sedimentary Facies and Sedimentology of the Late Quaternary Santa Barbara Basin, Site 893, edited by: Kennett, J. P., Baldauf, J. G., and Lyle, M., Proc. ODP, Sci. Results, 146, 295–308, 1995.

Berner, R. A.: A new geochemical classification of sedimentary environments, J. Sediment. Petrol., 51, 359–365, 1981.

CPD
10, 1223–1264, 2014

Berner, R. A. and Raiswell, R.: C/S method for distinguishing freshwater from marine sedimentary rocks, Geology, 12, 365–368, doi:10.1130/0091-7613(1984)12<365:CMFDFF>2.0.CO;2, 1984.
Bown, P. R. and Young, J. R.: Techniques, in Calcareous Nannofossil Biostratigraphy, edited by: Bown, P. R., Chapman & Hall, Cambridge, 16–28, 1998.
Burnett, J. A.: Upper Cretaceous, in Calcareous Nannofossil Biostratigraphy, edited by: Bown, P. R., Chapman & Hall, Cambridge, 132–199, 1998.
Chapman, M. R., Shackleton, N. J., and Chapman, M. R.: Evidence of 550-year and 1000-year cyclicities in North Atlantic circulation patterns during the Holocene, Holocene, 10, 287–291, doi:10.1191/095968300671253196, 2000.
Damon, P. E. and Sonett, C. P.: Solar and terrestrial components of the atmospheric C-14 variation spectrum, in: The Sun in Time, Vol. 1, edited by: Sonett, C. P., Giampapa, M. S., and Matthews, M. S., Tuscon, AZ, University of Arizona Press, 360–388 1991.
Dean, W. E. and Schwalb, A.: Holocene environmental and climatic change in the Northern Great Plains as recorded in the geochemistry of sediments in Pickerel Lake, South Dakota, Quaternary Int., 67, 5–20, 2000.
Dean, W., Anderson, R., Platt Bradbury, J., and Anderson, D.: A 1500-year record of climatic and environmental change in ElkLake, Minnesota I: Varve thickness and gray-scale density, J. Paleolimnol., 27, 287–299–299, doi:10.1023/A:1016062207440, 2002.
Dellmour, R. and Harzhauser, M.: The Iváò Canyon, a large Miocene canyon in the Alpine-Carpathian Foredeep, Mar. Petrol. Geol., 38, 83–94, 2012.
Di Rita, F.: A possible solar pacemaker for Holocene fluctuations of a salt-marsh in southern Italy, Quaternary Int., 288, 239–248, doi:10.1016/j.quaint.2011.11.030, 2013.
Domack, E., Leventer, A., Dunbar, R., Taylor, F., Brachfeld, S., and Sjunneskog, C.: ODP Leg 178 Scientific Party: chronology of the Palmer Deep site, Antarctic Peninsula: a Holocene palaeoenvironmental reference for the circum-Antarctic, Holocene, 11, 1–9, doi:10.1191/095968301673881493, 2001.
Erlykin, A. D., Sloan, T., and Wolfendale, A. W.: Correlations of clouds, cosmic rays and solar irradiation over the Earth, J. Atmos. Sol.-Terr. Phy., 72, 151–156, doi:10.1016/j.jastp.2009.11.002, 2010.
Flores, J. A., Sierro, F. J., and Raffi, I.: Evolution of the Calcareous Nannofossil Assemblage as A Response to the Paleoceanographic Changes in the Eastern Equatorial Pacific Ocean from 4 to 2 Ma (Leg 138, Sites 849 and 852), edited by: Pisias, N. G., Mayer, L. A., Janecek, T. R.,

CPD
10, 1223–1264, 2014

Palmer-Julson, A. A., and van Andel, T. H., Proc. ODP, Sci. Results, 138, 163–176, College Station, TX, 1995.
Fornaciari, E. and Rio, D.: Latest Oligocene to early middle Miocene quantitative calcareous nannofossil biostratigraphy in the Mediterranean region, Micropaleontology, 42, 1–36, 1996.
Fornaciari, E., Stefano, A. D., Rio, D., and Negri, A.: Middle Miocene quantitative calcareous nannofossil biostratigraphy in the Mediterranean region, Micropaleontology, 42, 37–63, 1996.
Frignani, M., Langone, L., Ravaioli, M., Sorgente, D., Alvisi, F., and Albertazzi, S.: Fine-sediment mass balance in the western Adriatic continental shelf over a century time scale, Mar. Geol., 222–223, 113–133, doi:10.1016/j.margeo.2005.06.016, 2005.
Galloway, J. M., Wigston, A., Patterson, R. T., Swindles, G. T., Reinhardt, E., and Roe, H. M.: Climate change and decadal to centennial-scale periodicities recorded in a late Holocene NE Pacific marine record: examining the role of solar forcing, Palaeogeogr. Palaeoclimatol. Palaeoecol., 386, 669–689, doi:10.1016/j.palaeo.2013.06.031, 2013.
Galović, I. and Young, J. R.: Revised taxonomy and stratigraphy of Middle Miocene calcareous nannofossils of the Paratethys, Micropaleontology, 58, 305–334, 2012.
Girone, A., Maiorano, P., Marino, M., and Kucera, M.: Calcareous plankton response to orbital and millennial-scale climate changes across the Middle Pleistocene in the western Mediterranean, Palaeogeogr. Palaeoclimatol. Palaeoecol., 392, 105–116, doi:10.1016/j.palaeo.2013.09.005, 2013.
Gleissberg, W.: A long-periodic fluctuation of the sun-spot numbers, Observatory, 62, 158–159, 1939.
Gradstein, F., Ogg, J., Schmitz, M., and Ogg, G. (Eds.): The Geologic Time Scale 2012, Elsevier, Boston, 2012.
Gray, L. J., Beer, J., Geller, M., Haigh, J. D., Lockwood, M., Matthes, K., Cubasch, U., Fleitmann, D., Harrison, G., Hood, L., Luterbacher, J., Meehl, G. A., Shindell, D., van Geel, B., and White, W.: Solar influences on climate, Rev. Geophys., 48, RG4001, doi:10.1029/2009RG000282, 2010.
Gross, M., Piller, W. E., Scholger, R., and Gitter, F.: Biotic and abiotic response to palaeoenvironmental changes at Lake Pannons' western margin (Central Europe, Late Miocene), Palaeogeogr. Palaeoclimatol. Palaeoecol., 312, 181–193, doi:10.1016/j.palaeo.2011.10.010, 2011.

CPD
10, 1223–1264, 2014

Grunert, P., Harzhauser, M., Rögl, F., Sachsenhofer, R. F., Gratzer, R., Soliman, A., and Piller, W. E.: Oceanographic conditions as a trigger for the formation of an Early Miocene (Aquitanian) Konservat-Lagerstätte in the Central Paratethys Sea, Palaeogeogr. Palaeoclimatol. Palaeoecol., 292, 425–442, doi:10.1016/j.palaeo.2010.04.001, 2010a.
Grunert, P., Soliman, A., Ćorić, S., Scholger, R., Harzhauser, M., and Piller, W. E.: Stratigraphic re-evaluation of the stratotype for the regional Ottnangian stage (Central Paratethys, middle Burdigalian), Newsl. Stratigr., 44, 1–16, doi:10.1127/0078-0421/2010/0001, 2010b.
Grunert, P., Soliman, A., Harzhauser, M., Müllegger, S., Piller, W. E., Roetzel, R., and Rögl, F.: Upwelling conditions in the Early Miocene Central Paratethys Sea, Geologica Carpathica, 61, 129–145, 2010c.
Grunert, P., Soliman, A., Ćorić, S., Roetzel, R., Harzhauser, M., and Piller, W. E.: Facies development along the tide-influenced shelf of the Burdigalian Seaway: an example from the Ottnangian stratotype (Early Miocene, middle Burdigalian), Mar. Micropaleontol., 84–85, 14–36, doi:10.1016/j.marmicro.2011.11.004, 2012.
Hammer, Ø.: Time series analysis with Past, Website of the Natural History Museum, University Oslo, 1–18 [online], available at: http://nhm2.uio.no/norlex/past/TimeseriesPast.pdf (last access: 12 August 2012), 2010.
Hammer, Ø., Harper, D. A. T., and Ryan, P. D.: PAST: paleontological statistics software package for education and data analysis, Palaeontol. Electron., 4, 1–9, 2001.
Haq, B. U.: Biogeographic history of Miocene calcareous nannoplankton and paleoceanography of the Atlantic Ocean, Micropaleontology, 26, 414–443, 1980.
Harzhauser, M. and Piller, W. E.: Benchmark data of a changing sea – palaeogeography, palaeobiogeography and events in the Central Paratethys during the Miocene, Palaeogeogr. Palaeoclimatol. Palaeoecol., 253, 8–31, doi:10.1016/j.palaeo.2007.03.031, 2007.
Harzhauser, M., Mandic, O., Kern, A. K., Piller, W. E., Neubauer, T. A., Albrecht, C., and Wilke, T.: Explosive demographic expansion by dreissenid bivalves as a possible result of astronomical forcing, Biogeosciences, 10, 8423–8431, doi:10.5194/bg-10-8423-2013, 2013.
Hohenegger, J. and Wagreich, M.: Time calibration of sedimentary sections based on insolation cycles using combined cross-correlation: dating the gone Badenian stratotype (Middle Miocene, Paratethys, Vienna Basin, Austria) as an example, Int. J. Earth Sci., 101, 339–349, doi:10.1007/s00531-011-0658-y, 2011.
Incarbona, A., Ziveri, P., Di Stefano, E., Lirer, F., Mortyn, G., Patti, B., Pelosi, N., Sprovieri, M., Tranchida, G., Vallefuoco, M., Albertazzi, S., Bellucci, L. G., Bonanno, A., Bonomo, S.,

CPD
10, 1223–1264, 2014

Censi, P., Ferraro, L., Giuliani, S., Mazzola, S., and Sprovieri, R.: The impact of the Little Ice Age onCoccolithophores in the Central Mediterranea Sea, Clim. Past, 6, 795–805, doi:10.5194/cp-6-795-2010, 2010.

Kern, A. K., Harzhauser, M., Piller, W. E., Mandic, O., and Soliman, A.: Strong evidence for the influence of solar cycles on a Late Miocene lake system revealed by biotic and abiotic proxies, Palaeogeogr. Palaeoclimatol. Palaeoecol., 329–330, 124–136, doi:10.1016/j.palaeo.2012.02.023, 2012.

Kern, A. K., Harzhauser, M., Soliman, A., Piller, W. E., and Mandic, O.: High-resolution analysis of upper Miocene lake deposits: evidence for the influence of Gleissberg-band solar forcing, Palaeogeogr. Palaeoclimatol. Palaeoecol., 370, 167–183, doi:10.1016/j.palaeo.2012.12.005, 2013.

Kristjánsson, J. E., Kristiansen, J., and Kaas, E.: Solar activity, cosmic rays, clouds and climate – an update, Adv. Space Res., 34, 407–415, doi:10.1016/j.asr.2003.02.040, 2004.

Kuypers, M. M. M., Lourens, L. J., Rijpstra, W. I. C., Pancost, R. D., Nijenhuis, I. A., and Sinninghe Damsté, J. S.: Orbital forcing of organic carbon burial in the proto-North Atlantic during oceanic anoxic event 2, Earth Planet. Sc. Lett., 228, 465–482, 2004.

Le Treut, H., Somerville, R., Cubasch, U., Ding, Y., Mauritzen, C., Mokssit, A., Peterson, T., and Prather, M.: Historical overview of climate change science, in: Climate Change 2007: The Physical Science Basis, Contribution of Working Group I to the Fourth Assessment Report of the Intergovernmental Panel on Climate Change, Vol. 1, edited by: Solomon, S., Qin, D., Manning, M., Chen, Z., Marquis, M., Averyt, K., Tignor, M. M. B., and Miller, H. L., Cambridge University Press, UK and New York, NY, USA, 94–127, 2007.

Lenz, O. K., Wilde, V., Riegel, W., and Harms, F.-J.: A 600 ky record of El Niño–Southern Oscillation (ENSO): evidence for persisting teleconnections during the Middle Eocene greenhouse climate of Central Europe, Geology, 38, 627–630, 2010.

Lindqvist, J. K. and Lee, D. E.: High-frequency paleoclimate signals from Foulden Maar, Waipiata Volcanic Field, southern New Zealand: an Early Miocene varved lacustrine diatomite deposit, Sediment. Geol., 222, 98–110, doi:10.1016/j.sedgeo.2009.07.009, 2009.

Martini, E.: Standard tertiary and quaternary calcareous nannoplankton zonation, in: Proceedings of the Second Planktonic Conference Roma 1970, Vol. 2, edited by: Farinacci, A., Edizioni Tecnoscienza, Rome, 739–785, 1971.

Maynard, J. B.: Extension of Berner's "New geochemical classification of sedimentary environments" to ancient sediments, J. Sediment. Petrol., 52, 1325–1331, 1982.

CPD
10, 1223–1264, 2014

Mertens, K. N. J. M., Lynn, M., Aycard, M., Lin, H.-L., and Louwye, S.: Coccolithophores as palaeoecological indicators for shifts of the ITCZ in the Cariaco Basin during the late Quaternary, J. Quaternary Sci., 24, 159–174, 2009.
Meyers, P. A. and Arnaboldi, M.: Trans-Mediterranean comparison of geochemical paleoproductivity proxies in a mid-Pleistocene interrupted sapropel, Palaeogeogr. Palaeoclimatol. Palaeoecol., 222, 313–328, 2005.
Negri, A. and Giunta, S.: Calcareous nannofossil paleoecology in the sapropel S1 of the eastern Ionian sea: paleoceanographic implications, Palaeogeogr. Palaeoclimatol. Palaeoecol., 169, 101–112, 2001.
Nehyba, S. and Petrová, P.: Karpatian sandy deposits in the southern part of the Carpathian Foredeep in Moravia, Bull. Czech Geol. Surv., 75, 53–66, 2000.
Ogurtsov, M. G., Nagovitsyn, Y. A., Kocharov, G. E., and Jungner, H.: Long-period cycles of the sun's activity recorded in direct solar data and proxies, Sol. Phys., 211, 371–394, doi:10.1023/A:1022411209257, 2002.
Okada, H. and Honjo, S.: The distribution of oceanic coccolithophorids in the Pacific, Deep-Sea Res., 20, 355–374, 1973.
Okada, H. and Wells, P.: Late Quaternary nannofossil indicators of climate change in two deep-sea cores associated with the Leeuwin Current off Western Australia, Palaeogeogr. Palaeoclimatol. Palaeoecol., 131, 413–432, 1997.
Paillard, D., Labeyrie, L., and Yiou, P.: Macintosh program performs time-series analysis, Eos Trans. AGU, 77, 379–379, doi:10.1029/96EO00259, 1996.
Patterson, R. T., Prokoph, A., and Chang, A.: Late Holocene sedimentary response to solar and cosmic ray activity influenced climate variability in the NE Pacific, Sediment. Geol., 172, 67–84, doi:10.1016/j.sedgeo.2004.07.007, 2004.
Patterson, R. T., Chang, A. S., Prokoph, A., Roe, H. M., and Swindles, G. T.: Influence of the Pacific Decadal Oscillation, El Niño-Southern Oscillation and solar forcing on climate and primary productivity changes in the northeast Pacific, Quatern. Int., 310, 124–139, doi:10.1016/j.quaint.2013.02.001, 2013.
Perch-Nielsen, K.: Cenozoic calcareous nanofossils, in: Plankton Stratigraphy, Vol. 1, edited by: Bolli, H. M., Saunders, J. B., and Perch-Nielsen, K., Cambridge University Press, Cambridge, 427–554, 1985a.
Perch-Nielsen, K.: Mesozoic calcareous nannofossils, in: Plankton Stratigraphy, Vol. 1, Planktic Foraminifera, Calcareous Nannofossils and Calpionellids, edited by: Bolli, H. M., Saun-

CPD
10, 1223–1264, 2014

ders, J. B., and Perch-Nielsen, K., Cambridge University Press, Cambridge, 329–426, 1985b.
Piller, W. E., Harzhauser, M., and Mandic, O.: Miocene Central Paratethys stratigraphy – current status and future directions, Stratigraphy, 4, 71–88, 2007.
Raspopov, O. M., Dergachev, V. A., Esper, J., Kozyreva, O. V., Frank, D., Ogurtsov, M. G., Kolström, T., and Shao, X.: The influence of the de Vries (~ 200-year) solar cycle on climate variations: results from the Central Asian Mountains and their global link, Palaeogeogr. Palaeoclimatol. Palaeoecol., 259, 6–16, 2008.
Roetzel, R. and Schnabel, W.: Molasse, Waschbergzone, Paläogen und Neogen auf der Böhmischen Masse, in: Legende und Kurzerläuterung der Geologischen Karte von Niederösterreich, 1 : 200.000, edited by: Schnabel, W., 23–30, Geologische Bundesanstalt, Vienna, 2002.
Roetzel, R., Ćorić, S., Galović, I., and Rögl, F.: Early Miocene (Ottnangian) coastal upwelling conditions along the southeastern scarp of the Bohemian Massif (Parisdorf, Lower Austria, Central Paratethys), Beitr. Paläont., 30, 387–413, 2007.
Rohling, E. J.: Review and new aspects concerning the formation of eastern Mediterranean sapropels, Mar. Geol., 122, 1–28, doi:10.1016/0025-3227(94)90202-X, 1994.
Sanchez-Cabeza, J. A., Masqué, P., Ani-Ragolta, I., Merino, J., Frignani, M., Alvisi, F., Palanques, A., and Puig, P.: Sediment accumulation rates in the southern Barcelona continental margin (NW Mediterranean Sea) derived from ^{210}Pb and ^{137}Cs chronology, Prog. Oceanogr., 44, 313–332, 1999.
Santos, F., Gómez-Gesteira, M., deCastro, M., and Álvarez, I.: Upwelling along the western coast of the Iberian Peninsula: dependence of trends on fitting strategy, Clim. Res., 48, 213–218, doi:10.3354/cr00972, 2011.
Schimmelmann, A., Lange, C. B., and Meggers, B. J.: Palaeoclimatic and archaeological evidence for a ~ 200 yr recurrence of floods and droughts linking California, Mesoamerica and South America over the past 2000 yr, Holocene, 13, 763–778, doi:10.1191/0959683603hl661rp, 2003.
Schulz, M. and Mudelsee, M.: REDFIT: estimating red-noise spectra directly from unevenly spaced paleoclimatic time series, Comput. Geosci., 28, 421–426, 2002.
Schwabe, H. and Schwabe, H.: Sonnen-Beobachtungen im Jahre 1843, Astron. Nachr., 21, 234–235, 1844.

CPD
10, 1223–1264, 2014

Sokal, R. R. and Rohlf, F. J.: Biometry, 3rd edn., W. H. Freeman and Company, New York, 1995.

Solanki, S. K., Usoskin, I. G., Kromer, B., Schüssler, M., and Beer, J.: Unusual activity of the Sun during recent decades compared to the previous 11,000 yr, Nature, 431, 1084–1087, doi:10.1038/nature02995, 2004.

Spezzaferri, S. and Ćorić, S.: Ecology of Karpatian (Early Miocene) foraminifers and calcareous nannoplankton from Laa an der Thaya, Lower Austria: a statistical approach, Geol. Carpath., 52, 361–374, 2001.

Spezzaferri, S., Ćorić, S., Hohenegger, J., and Rögl, F.: Basin-scale paleobiogeography and paleoecology: an example from Karpatian (Latest Burdigalian) benthic and planktonic foraminifera and calcareous nannofossils from the Central Paratethys, Geobios, 35, 241–256, 2002.

Stanley, S. M., Ries, J. B., and Hardie, L. A.: Seawater chemistry, coccolithophore population growth, and the origin of Cretaceous chalk, Geology, 33, 593–596, doi:10.1130/G21405.1, 2005.

Stax, R. and Stein, R.: Data Report: Organic Carbon and Carbonate Records from Detroit Seamount and Patton-Murray Seamount: Results from Sites 882 and 887 (North Pacific Transect), edited by: Rea, D. K., Basov, L. A., Scholl, D. W., and Allan, J. F., Proc. ODP, Sci. Results, 145, 645–655, College Station, TX, 1995.

Stein, R. and Rack, F. R.: A 160,000-year high-resolution record of quantity and composition of organic carbon in the Santa Barbara Basin (Site 893), edited by: Kennett, J. P., Baldauf, J. G., and Lyle, M., Proc. ODP, Sci. Results, 146, 125–138, 1992.

Stuiver, M. and Braziunas, T. F.: Sun, ocean, climate and atmospheric $^{14}CO_2$: an evaluation of causal and spectral relationships, Holocene, 3, 289–305, doi:10.1177/095968369300300401, 1993.

Stuiver, M., Grootes, P. M., and Braziunas, T. F.: The GISP2 $\delta^{18}O$ climate record of the past 16,500 years and the role of the sun, ocean, and volcanoes, Quaternary Res., 44, 341–354, doi:10.1006/qres.1995.1079, 1995.

Svabenicka, L., Ćorić, S., Andreyeva-Grigorovich, A. S., Halasova, E., Marunteanu, M., Nagymarosy, A., and Oszczypko-Clowes, M.: Central paratethys karpatian calcareous nannofossils, in: The Karpatian – a Lower Miocene Stage of the Central Paratethys, edited by: Brzobohaty, R., Cicha, I., Kovác, M., and Rögl, F., Masaryk University, Brno, 151–167, 2003.

CPD
10, 1223–1264, 2014

Svensmark, H. and Friis-Christensen, E.: Variation of cosmic ray flux and global cloud coverage – a missing link in solar-climate relationships, J. Atmos. Sol.-Terr. Phy., 59, 1225–1232, doi:10.1016/S1364-6826(97)00001-1, 1997.

Taricco, C., Ghil, M., Alessio, S., and Vivaldo, G.: Two millennia of climate variability in the Central Mediterranean, Clim. Past, 5, 171–181, doi:10.5194/cp-5-171-2009, 2009.

Thunell, R. C., Tappa, E., and Anderson, D. M.: Sediment fluxes and varve formation in Santa Barbara Basin, offshore California, Geology, 23, 1083–1086, doi:10.1130/0091-7613(1995)023<1083:SFAVFI>2.3.CO;2, 1995.

Varol, O.: Palaeogene, in: Calcareous Nannofossil Biostratigraphy, edited by: Bown, P. R., Chapman & Hall, Cambridge, 200–224, 1998.

Villinski, J. C. and Domack, E.: Temporal changes in sedimentary organic carbon $\delta^{13}C$ from the Ross Sea, Antarctica: Inferred changes in ecosystems and climate, American Geophysical Union, Abstracts of Ocean Science Meeting, 1998.

Wade, B. S. and Bown, P. R.: Calcareous nannofossils in extreme environments: the Messinian Salinity Crisis, Polemi Basin, Cyprus, Palaeogeogr. Palaeoclimatol. Palaeoecol., 233, 271–286, doi:10.1016/j.palaeo.2005.10.007, 2006.

Wagner, G., Beer, J., Masarik, J., Muscheler, R., Kubik, P. W., Mende, W., Laj, C., Raisbeck, G. M., and Yiou, F.: Presence of the Solar de Vries Cycle (~ 205 yr) during the Last Ice Age, Geophys. Res. Lett., 28, 303–306, doi:10.1029/2000GL006116, 2001.

Weedon, G. P.: Time-Series Analysis and Cyclostratigraphy: examining Stratigraphic Records of Environmental Cycles, Cambridge University Press, 2003.

Wolf, R.: Astronomische Mitteilungen der Eidgenössischen Sternwarte Zurich, Astronomische Mittheilungen LXXIX, 8, 317–364, 1892.

Yin, Z. Q., Ma, L. H., Han, Y. B., and Han, Y. G.: Long-term variations of solar activity, Chinese Sci. Bull., 52, 2737–2741–2741, doi:10.1007/s11434-007-0384-9, 2007.

Young, J. R.: Neogene, in Calcareous Nannofossil Biostratigraphy, edited by: Bown, P. R., 225–265, Chapman & Hall, Cambridge, 1998.

Young, J. R., Bown, P. R., and Lees, J. A. (Eds.): Nannotax website, International Nannoplankton Association, [online], available at: http://nannotax.org (last access: 14 March 2013), 2013.

CPD
10, 1223–1264, 2014

Table 1. Overview of the 9 studied proxies. Table shows highest and lowest values, average content (arithmetic mean) as well as the standard deviation.

	max	min	Average	σ (pp)
calcium carbonate (wt%)	22.7	13.02	16.44	1.48
sulphur (wt%)	0.57	0.03	0.33	0.05
TOC (wt%)	0.92	0.53	0.78	0.09
Coccolithus pelagicus (%)	46.62	22.7	34.52	4.89
Cyclicargolithus floridanus (%)	17.76	2.96	8.57	3.22
Reticulofenestra haqii (%)	13.04	1.32	5.76	2.5
Reticulofenestra minuta (%)	26.67	3.3	12.48	4.93
Reticulofenestra pseudoumbilicus (%)	5.45	0	2.18	1.2
Autochthonous taxa < 1 % (%)	7.52	0.32	4.06	1.61
allochthonous taxa (%)	48.52	22.44	32.44	5.37

CPD
10, 1223–1264, 2014

Table 2. Overview of the setting used in REDFIT for the 9 studied proxies.

	Window	Segments	Oversample
calcium carbonate	Blackman–Harris	1	4
sulphur	Blackman–Harris	2	4
TOC	Welch	3	4
Coccolithus pelagicus	Blackman–Harris	1	4
Cyclicargolithus floridanus	Blackman–Harris	3	4
Reticulofenestra haqii	Welch	2	4
Reticulofenestra minuta	Welch	2	3
Reticulofenestra pseudoumbilicus	Welch	3	2
allochthonous taxa	Rectangle	4	4

CPD
10, 1223–1264, 2014

Table 3. Summary of results of the REDFIT analysis for the 9 analysed proxies. Table shows the detected frequencies, their confidence intervals (Monte-Carlo corrected), as well as the resulting periodicity in mm. Periodicities in mm were then transformed into periodicities in years using a sedimentation rate of 575 mm kyr^{-1} (best-fit adjustment to known solar cycles).

	Frequencies (mm^{-1})	Confidence (% MoCa AR1)	Periodicity (mm)	Periodicity (575 mm kyr^{-1})
calcium carbonate	0.0065326	> 90 %	153.08	266.23
	0.0108826	> 99 %	91.84	159.72
	0.025768	< 80 %	38.81	67.50
	0.0323	< 80 %	30.96	53.84
sulphur	0.0079843	> 99 %	125.25	217.83
	0.022501	> 99 %	44.44	77.29
	0.027582	> 95 %	36.26	63.06
TOC	0.0083473	> 99 %	119.8	208.35
	0.030123	> 90 %	33.2	57.74
Coccolithus pelagicus	0.0036292	> 99 %	275.54	479.20
	0.0083472	> 99 %	119.8	208.35
	0.017057	> 90 %	58.63	101.97
Cyclicargolithus floridanus	0.0043551	> 99 %	229.61	399.32
Reticulofenestra haqii	0.015351	> 90 %	65.14	113.29
	0.023575	> 90 %	42.41	73.76
Reticulofenestra minuta	0.015351	> 90 %	65.14	113.29
	0.023392	> 90 %	42.74	74.33
Reticulofenestra pseudoumbilicus	0.0058068	> 95 %	172.21	299.50
	0.039196	> 90 %	25.51	44.37
	0.01742	< 80 %	57.41	99.84
allochthonous taxa	0.0138	> 90 %	77.61	134.97
	0.027608	> 80 %	45.28	78.75
	0.022086	> 80 %	36.22	62.99

CPD
10, 1223–1264, 2014

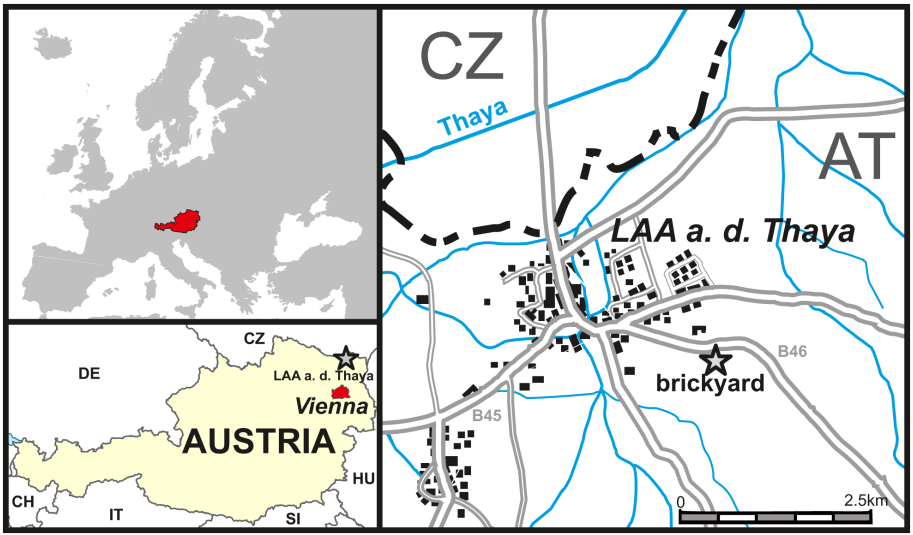

Fig. 1. Map showing the position of the studied outcrop near Laa and der Thaya in Lower Austria (after Auer et al., 2014).

CPD
10, 1223–1264, 2014

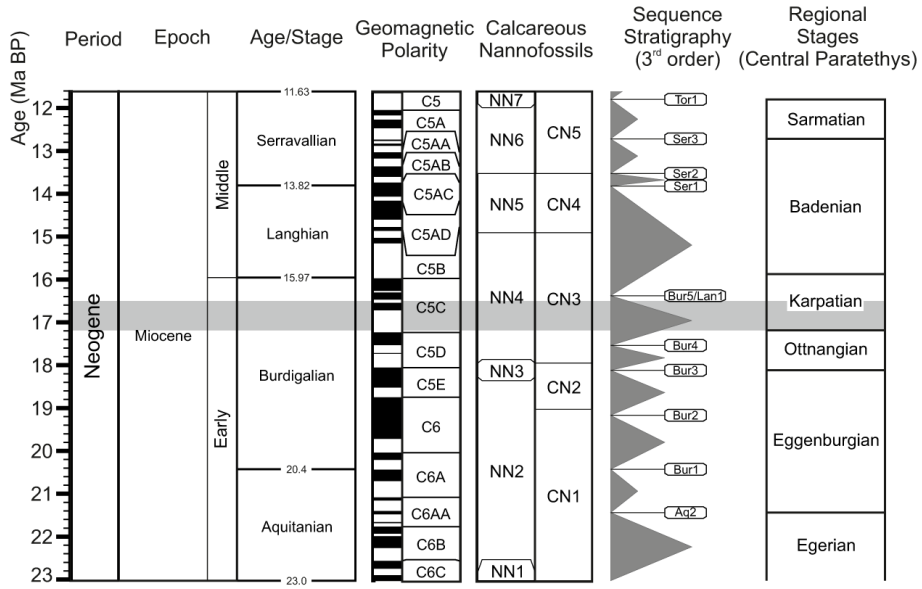

Fig. 2. Stratigraphic table of the Early to Middle Miocene, showing global geochronology after Gradstein et al. (2012) and references therein. Regional stages of the Central Paratethys after Piller et al. (2007), with updated ages for the Ottnangian and Karpatian after Grunert et al. (2010) and Dellmour and Harzhauser (2012). Grey bar indicates the stratigraphic position of the Laa Formation (after Auer et al., 2014).

CPD
10, 1223–1264, 2014

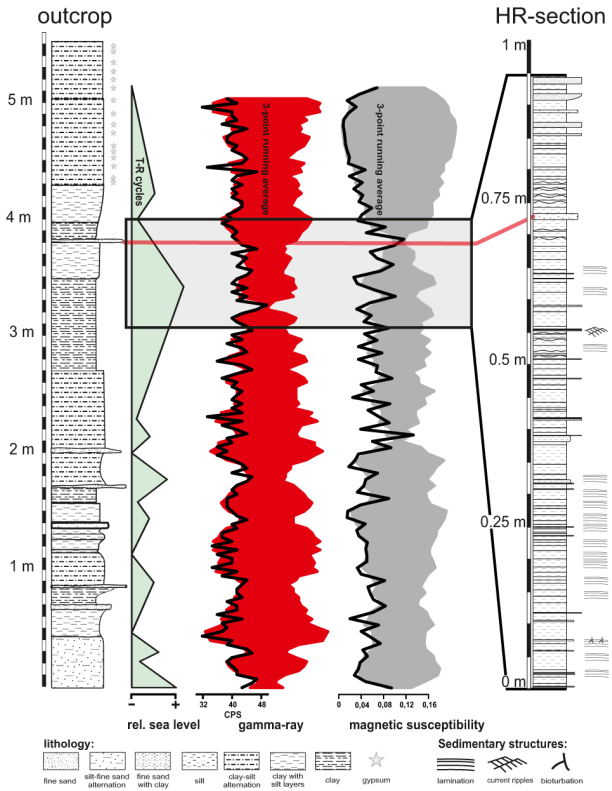

Fig. 3. Lithologs of the 5.5 m sedimentary succession and the high-resolution (HR) section. Position of the HR-section within the succession is marked by the grey rectangle, red line denotes a distinct marker layer that was used as a tie point. Relative sea level was reconstructed using gamma-ray logs. Gamma-ray log (in CPS) and magnetic susceptibility of the succession are shown as black lines. A three point running mean for both logs was plotted as a mirrored column.

CPD
10, 1223–1264, 2014

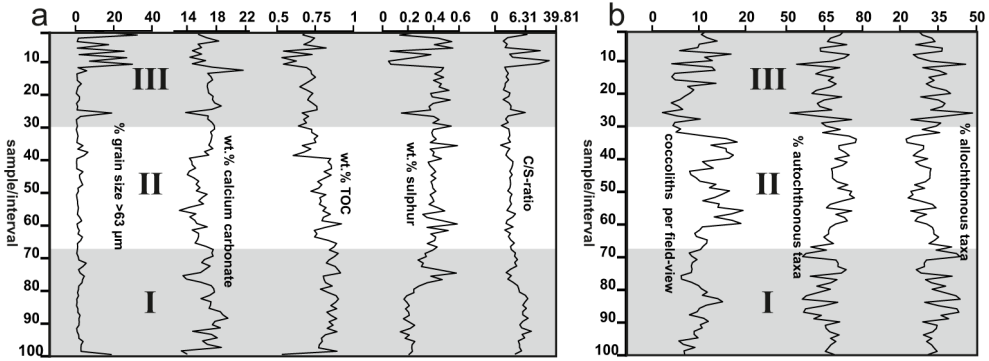

Fig. 4. Sedimentological (% of grains > 63 µm) and geochemical paramters (calcium carbonate, organic carbon, sulphur and C/S-ratio) of the high resolution section **(a)**. Coccolith abundances are shown as coccoliths encountered per field-view of the light microscope and the abundance of autochthonous and allochthonous specimens in % **(b)**. Three basic depositional intervals (I-III) were defined based on a simple visual evaluation of the gathered datasets.

CPD
10, 1223–1264, 2014

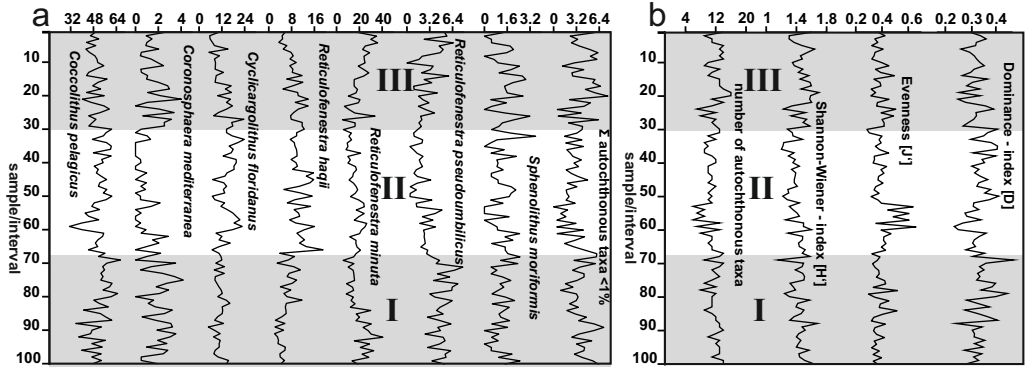

Fig. 5. Relative abundances of autochthonous coccolith taxa > 1 % as well as the abundance of autochthonous taxa < 1 %, normalized to 100 %, within each sample of the high- resolution section **(a)**. Diversity indices show the amount of autochthonous taxa, the Shannon–Wiener index, species evenness and the Dominance index of the studied samples **(b)**. The three intervals (I–III) show the depositional episodes defined by visual evaluation of the gathered datasets.

CPD
10, 1223–1264, 2014

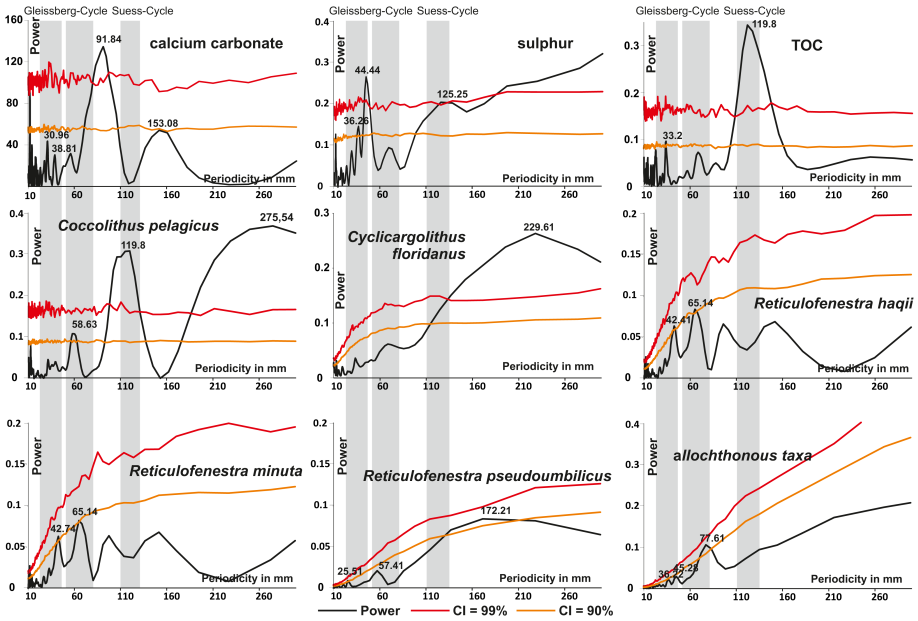

Fig. 6. Periodograms of the nine investigated geochemical and palaeoecological proxies showing their respective periodicities in mm calculated using REDFIT. Grey bars represent the reported periodicities of the Lower- and Upper-Gleissberg cycle, and the Suess/de Vries-Cycle.

CPD
10, 1223–1264, 2014

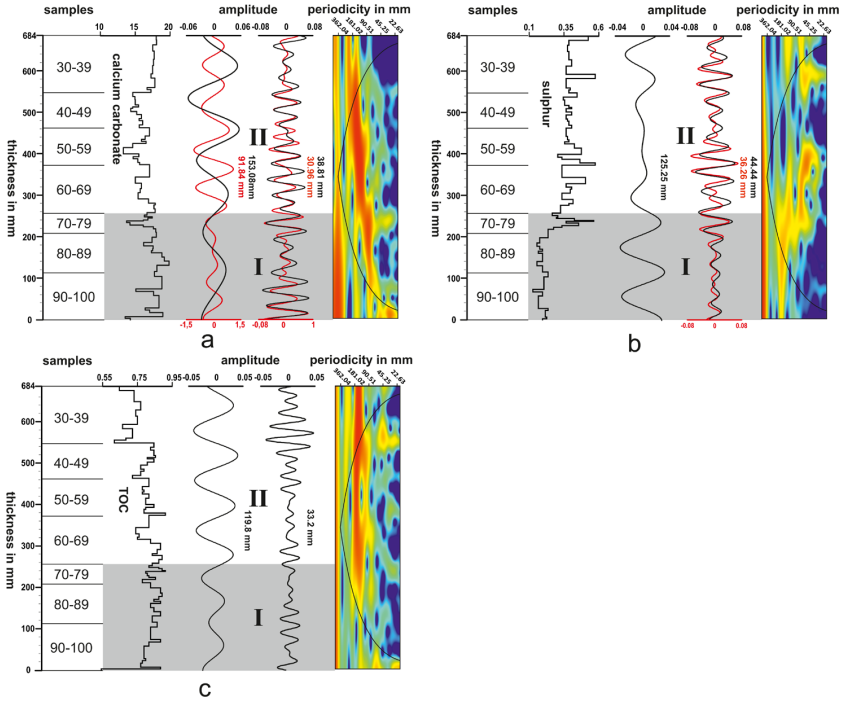

Fig. 7. Geochemical datasets (calcium carbonate, sulphur and TOC): data was transformed to reflect thicknesses of the sampled layers and filtered according to the periodicities detected by REDFIT. Gaussian filters applied to the periodicities use a bandwidth of 25 % of the filtered frequency. Wavelet spectra were used to evaluate the frequencies for spectral shifts; red areas of the wavelet indicate stronger amplitudes.

CPD
10, 1223–1264, 2014

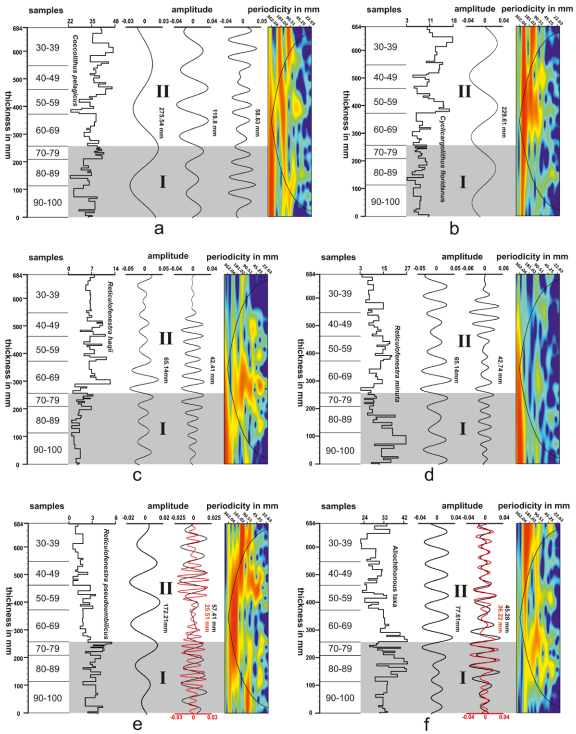

Fig. 8. Palaeobiological proxies (**a** *Coccolithus pelagicus*, **b** *Cyclicargolithus floridanus*, **c** *Reticulofenestra haqii*, **d** *Reticulofenestra minuta*, **e** *Reticulofenestra pseudoumbilicus* and **f** allochthonous taxa): data was transformed to reflect thicknesses of the sampled layers and filtered according to the periodicities detected by REDFIT. Gaussian filters applied to the periodicities use a bandwidth of 25 % of the filtered frequency. Wavelet spectra were used to evaluate the frequencies for spectral shifts; red areas of the wavelet indicate stronger amplitudes.

CPD
10, 1223–1264, 2014

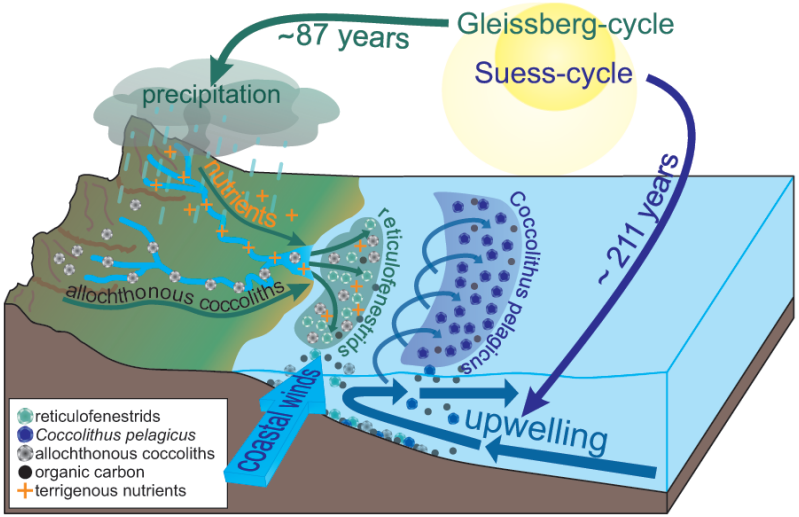

Fig. 9. Model depicting the Suess and Gleissberg cycles and the dominant influence they had on different palaeoenvironmental systems. The (combined upper ~ 113 yr and lower ~ 65 yr) Gleissberg cycle exerts control on precipitation, which in turn controls freshwater and terrigenous material input as well as nutrient influx from the hinterland, and variations in the abundance of reticulofenestrids. The Suess cycle (~ 211 yr) in turn exerts control over local coastal upwelling, as well as the amount auf *Coccolithus pelagicus*. Both cycles are reflected in primary productivity proxies, caused by the export of organic matter from both systems to the ocean floor.

CPD
10, 1223–1264, 2014